

ELECTRONIC SUPPLEMENTARY MATERIAL

Model-based scale-up and reactor design for solvent-free synthesis of an ionic liquid in a millistructured flow reactor

Sebastian Schwolow,[†] Benedikt Mutsch,[†] Norbert Kockmann,[‡] Thorsten Röder^{†,*}

[†] Mannheim University of Applied Sciences, Institute of Chemical Process Engineering,
Paul-Wittsack-Straße 10, 68163 Mannheim, Germany

[‡] TU Dortmund University, Biochemical and Chemical Engineering, Equipment Design,
Emil-Figge-Straße 68, 44227 Dortmund, Germany

* **Corresponding author.** Tel.: +49 621 292 6800

E-mail address: t.roeder@hs-mannheim.de.

Table S1 Structural elements of the flow channel on the reaction side of the plate reactor/heat exchanger

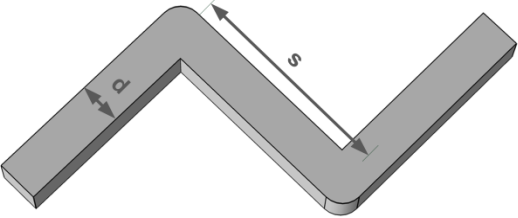
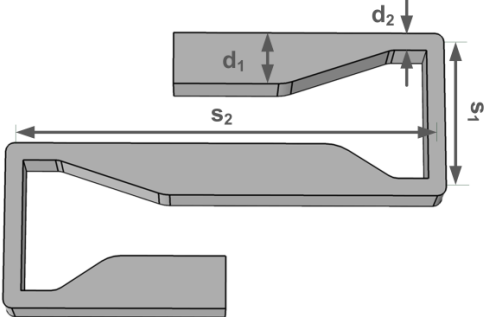
Structure I	Structure II	Structure III
$d = 1 \text{ mm}$ $s = 5 \text{ mm}$	$d_1 = 2 \text{ mm} / d_2 = 1 \text{ mm}$ $s_1 = 5.4 \text{ mm}$ $s_2 = 19 \text{ mm}$	$d_1 = 3 \text{ mm} / d_2 = 1 \text{ mm}$ $s_1 = 8.2 \text{ mm}$ $s_2 = 24 \text{ mm}$
		

Table S2 Specifications for the different channel sections on the applied plate reactor/heat exchanger shown in Fig. 4

	Mixer	Preheating sections	Residence time section 1	Residence time section 2
Structural element	Arrowhead	I	I	II
Cross-sectional area [mm ²]	0.5×0.5	1×1	1×1	2×2
Channel volume [mL]	< 0.01	$0.2 / 0.2 / 0.1$	1.88	1.75
Surface/volume ratio [m ⁻¹]	8000	4000	4000	2000

	Residence time section 3	Heat carrier channel
Structural element	III	-
Cross-sectional area [mm ²]	3×3	3×10
Channel volume [mL]	9.43	95
Surface/volume ratio [m ⁻¹]	1333	867

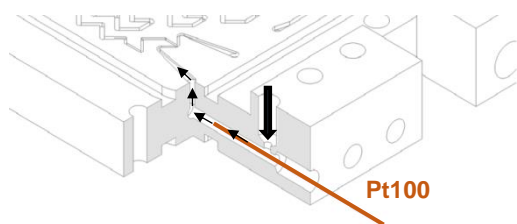


Fig. S1 Location of the thermometer (Pt100) for temperature measurements of the in- and outflowing fluids in the plate heat exchanger/reactor

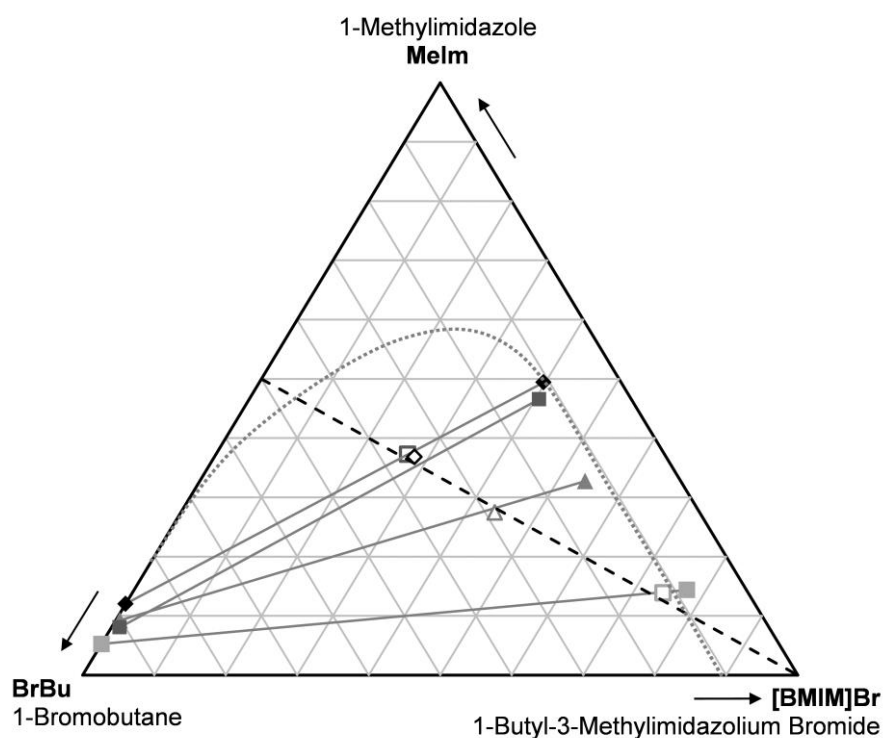


Fig. S2 Ternary phase diagram with the experimentally determined mole fractions for the two liquid phases formed during the [BMIM]Br synthesis. Open symbols represent the overall product composition (determined from analyses of the quenched product); filled symbols represent the composition of the single phases (determined from analyses after phase separation). The theoretical reaction progress for a reaction with equimolar reactant ratio is depicted by the dashed line. The dotted bimodal curve is a rough estimation of the separation between the single-phase region (above the curve) and the two-phase region (below the curve).

Calculation of phase-specific concentrations and phase volumes

Alkylation of 1-methylimidazole (MeIm) by 1-bromobutane (BrBu) follows a second-order rate equation.¹ Thus, the reaction rate r_{rp} based on the volume of the reaction phase (rp) can be expressed as follows:

$$r_{rp} = k c_{MeIm,rp} c_{BrBu,rp} \quad (S1)$$

The temperature dependency of the reaction rate constant k is given by the Arrhenius equation (Equation S2).²

$$k = A_0 e^{\left(\frac{-E_A}{RT}\right)} \quad (S2)$$

The reaction rate based on the total volume can be obtained by applying the ratio of the reaction phase and total flow rates as a correction factor (Equation S3)

$$r = r_{rp} \cdot \frac{\dot{V}_{rp}}{\dot{V}_{ges}} \quad (S3)$$

Conversion and temperature profiles can be determined with differential equations (Equations S4–S6) that describe an ideal plug flow reactor.

$$\frac{dX_{MeIm}}{dz} = \frac{r}{c_{MeIm,0} u} \quad (S4)$$

$$\frac{d\dot{n}_{MeIm,rp}}{dz} = \frac{\dot{V}_{rp}}{u} \left(-r_{rp} + k_l a (c_{MeIm,rp}^* - c_{MeIm,rp}) \right) \quad (S5)$$

$$\frac{dT}{dz} = \frac{1}{\rho c_p u} \left(r(-\Delta H_R) + \frac{4k_w}{d_h} (T_w - T) \right) \quad (S6)$$

Equation S5 enables calculation of the phase ratio based on the mass balance. All mass and flow rates of the two phases can be derived from $\dot{n}_{MeIm,rp}$ using the following equations:

$$\dot{n}_{MeIm,pp} = \dot{n}_{MeIm,ges} - \dot{n}_{MeIm,rp} \quad (S7)$$

$$\dot{V}_{rp} = \dot{V}_{MeIm,rp} + \dot{V}_{BrBu} = \frac{M_{MeIm}}{\rho_{MeIm}} \dot{n}_{MeIm,rp} + \dot{V}_{BrBu} \quad (S8)$$

$$\dot{V}_{pp} = \dot{V}_{MeIm,pp} + \dot{V}_{[BMIM]Br} = \frac{M_{MeIm}}{\rho_{MeIm}} (\dot{n}_{MeIm,ges} - \dot{n}_{MeIm,rp}) + \dot{V}_{[BMIM]Br} \quad (S9)$$

The flow rates in Equations S8–S9 result from the relationship $\dot{V}_i = (M_i/\rho_i)\dot{n}_i$, and the flow rates \dot{n}_i can be determined from the MeIm conversion via the mass balance.³

$$\dot{n}_{MeIm,ges} = \dot{n}_{MeIm,0}(1 - X_{MeIm}) \quad (S10)$$

$$\dot{n}_{BrBu} = \dot{n}_{BrBu,0} - \dot{n}_{MeIm,0} X_{MeIm} \quad (S11)$$

$$\dot{n}_{Br[BMIM]} = \dot{n}_{MeIm,0} X_{MeIm} \quad (S12)$$

The distribution coefficient K_p is used to determine the equilibrium concentration $c_{MeIm,rp}^*$ in Equation S5 as follows:

$$K_p = \frac{c_{MeIm,pp}}{c_{MeIm,rp}} = \frac{\dot{n}_{MeIm,pp} \dot{V}_{rp}}{\dot{n}_{MeIm,rp} \dot{V}_{pp}} \quad (S13)$$

Equations S7–S12 are combined to give Equation S14, which can be used to calculate the distribution coefficient.

$$K_p = \frac{(\dot{n}_{MeIm,ges} - \dot{n}_{MeIm,rp}) \left(\frac{M_{MeIm}}{\rho_{MeIm}} \dot{n}_{MeIm,rp} + \dot{V}_{BrBu} \right)}{\dot{n}_{MeIm,rp} \left(\frac{M_{MeIm}}{\rho_{MeIm}} (\dot{n}_{MeIm,ges} - \dot{n}_{MeIm,rp}) + \dot{V}_{[BMIM]Br} \right)} \quad (S14)$$

Equation S14 is a quadratic equation that can be solved for $\dot{n}_{MeIm,rp}$.

$$\dot{n}_{MeIm,rp} = \frac{-b + \sqrt{b^2 - 4ac}}{2a}$$

$$a = \frac{M_{MeIm}}{\rho_{MeIm}} (1 - K_p)$$

$$b = \frac{M_{MeIm}}{\rho_{MeIm}} \dot{n}_{MeIm,ges} (K_p - 1) + K_p \dot{V}_{[BMIM]Br} + \dot{V}_{BrBu}$$

$$c = -\dot{V}_{BrBu} \dot{n}_{MeIm,ges} \quad (S15)$$

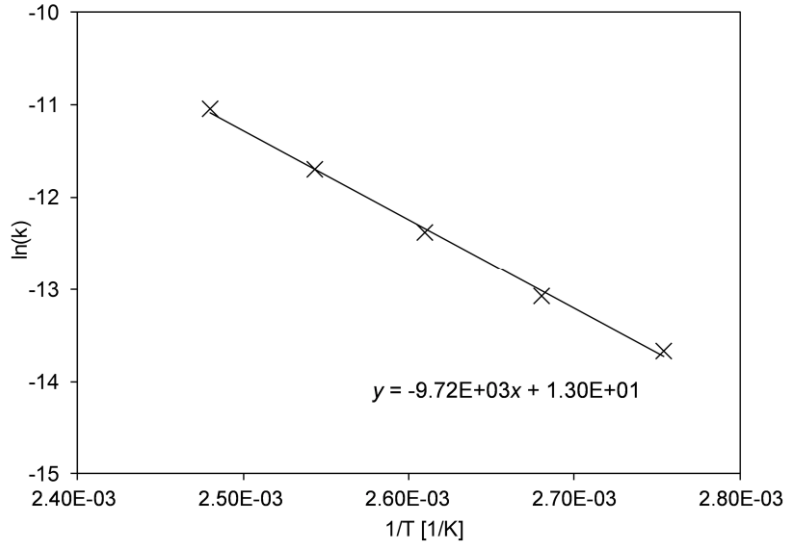


Fig. S3 Arrhenius plot for determining the reaction kinetic parameters (E_A and A_0 , Equation S2) in the kinetic model for solvent-free [BMIM]Br synthesis

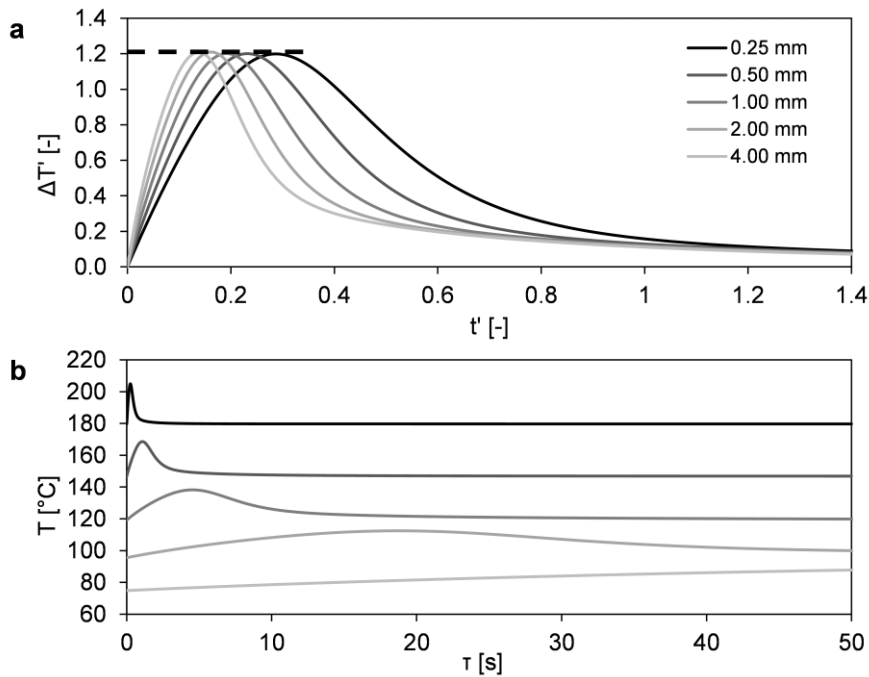


Fig. S4 Simulated axial temperature profiles with the maximum dimensionless temperature increase ($\Delta T'_{\max} = 1.2$) for different hydraulic channel diameters. a) Dimensionless temperature difference (Equation 1) versus dimensionless time $t' = t/t_r$. b) Reactor temperature versus hydrodynamic residence time

Computational Fluid Dynamics (CFD) simulations for channel design optimization

The design of the structural elements in the reaction channels of the millistructured plate reactor is based on an optimization by CFD simulations. In Fig. S5, this is illustrated exemplarily for the structural element III (Table S1) in the 3-mm channel of the reactor. By simulating single phase flow in a simple 3 mm zigzag structure at a flow rate of 10 mL min^{-1} , dead zones in the 90° flow redirection regions can be visualized (Fig. S5a). If the channel width in these regions is narrowed, this effect can be significantly reduced (Fig. S5b). A simulation of radial mixing in both structural elements is compared in Fig. S6 and Fig. S7. For these simulations, a segregated concentration profile was defined for the cross-section at the inlet ($c = 1 \text{ mol L}^{-1}$ at a central surface area of $1.5 \times 1.5 \text{ mm}^2$). The remaining segregation at the outlet cross-sections was compared for evaluation of the radial mixing efficiency. It is to be noted that the focus of the simulations was on the relative comparison of the performance of the different structural elements. Because a grid-invariant solution could not be ensured, the results are partially affected by numerical diffusion.

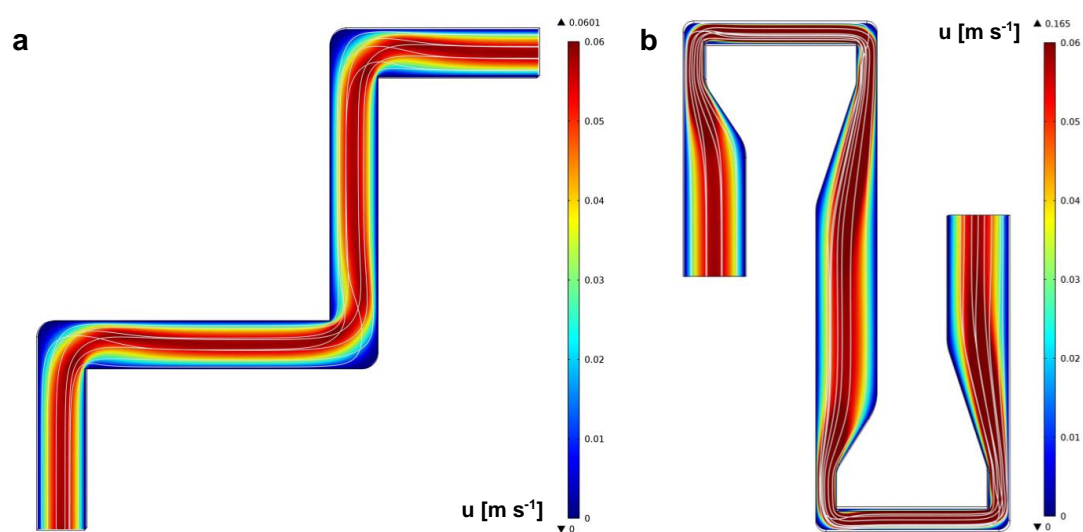


Fig. S5 Streamlines and visualization of the flow velocity in the reaction channel with a cross-sectional area of $3 \times 3 \text{ mm}^2$ (cut plane at channel height $h = 1.5 \text{ mm}$); a) Zigzag structure; b) Optimized channel geometry (structure III, see Table S1)

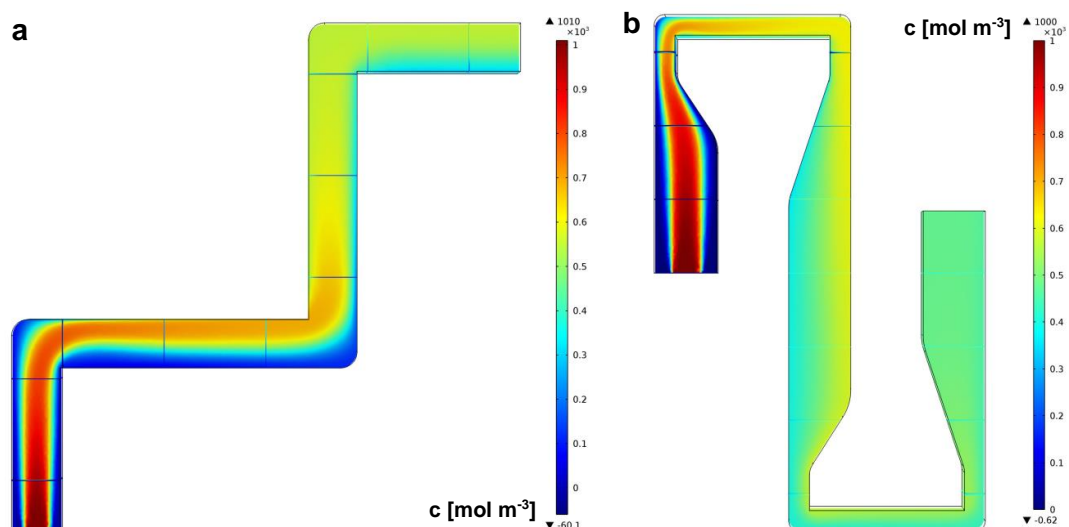


Fig. S6 Concentration profiles in the reactor channel with a cross-sectional area of $3 \times 3 \text{ mm}^2$ (cut plane at channel height $h = 1.5 \text{ mm}$, inlet concentration $c = 1 \text{ mol L}^{-1}$ in a central cross-sectional area of $1.5 \times 1.5 \text{ mm}^2$); a) Zigzag structure; b) Optimized channel geometry (structure III, see Table S1)

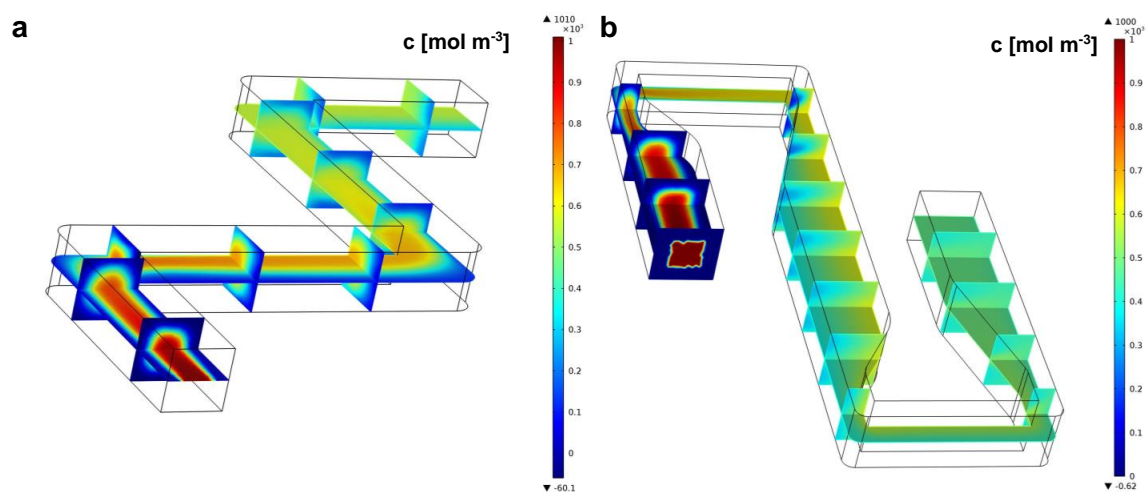


Fig. S7 Concentration profiles in the reactor channel with a cross-sectional area of $3 \times 3 \text{ mm}^2$ (cut planes at channel height $h = 1.5 \text{ mm}$ and various channel lengths, inlet concentration $c = 1 \text{ mol L}^{-1}$ in a central cross-sectional area of $1.5 \times 1.5 \text{ mm}^2$); a) Zigzag structure; b) Optimized channel geometry (structure III, see Table S1)

Experimental characterization of the mixing performance

The mixing performance in the microreactor setup and in the milled mixers of the millistructured plate reactor was characterized by an experimental approach with competitive test reactions. The chosen test reaction, a diazo coupling, is one of several mixing sensitive test reactions that were described by Baldyga, Bourne, and co-workers⁴⁻⁶. In a first quasi-instantaneous reaction of 1-naphthol (A) and diazotized sulphanic acid (B), isomeric monoazo dyes 2-[(4'-sulphophenyl)azo]-1-naphthol (o-R) and 4-[(4'-sulphophenyl)azo]-1-naphthol (p-R) are formed (S16 and S17). Subsequently, their secondary couplings produce one bisazo dye (2,4-bis[(4'-sulphophenyl)azo]-1-naphthol, S), in a fast, but comparatively slower reaction (S18 and S19). The shorter the mixing time in the reactor after contacting both reactant solutions, the lower is the yield of the bisazo dye (Y_S). For the detailed reaction scheme and kinetic aspects, see Bourne et al.⁵ and Baldyga et al.⁶ Experimental details of the characterization approach can be found in a previous publication by some of the authors⁷.



Fig. S8 shows a comparison of the arrowhead mixer in the microreactor setup (0.5 mm inner diameter, circular cross-section, 10 μm frit in the mixing channel) with the milled arrowhead-mixer in the plate reactor (0.5 mm \times 0.5 mm, quadratic cross-section, followed by a 1 mm zigzag channel, see Fig. 4). Similar values for Y_S were obtained for both the commercially available mixer (IDEX Health & Science, Oak Harbor, WA, USA) and the milled arrowhead mixer. At the aimed flow rate of 10 mL min^{-1} , a low bisazo yield ($Y_S < 5\%$) indicated excellent mixing performance (mixing times $t_R \ll 1$ s, see Baldyga et al.⁶ for the characteristic mixing times of the test reactions). The comparison with a 1 mm mixer in a similar prototype plate reactor demonstrated a significant increase of mixing performance due to the decreased channel diameter.

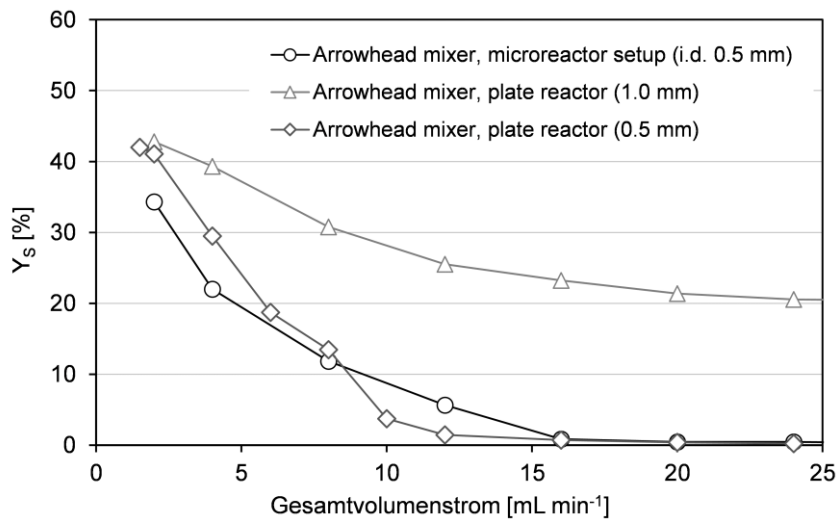


Fig. S8 Experimental results of the bisazo dye yield Y_S as a function of the total flow rate for the different investigated micromixers; a decrease of Y_S indicates an increase in the mixing performance.

NOTATION

A_0	frequency factor of the reaction, n th-order ($L^{n-1} \text{ mol}^{1-n} \text{ s}^{-1}$)
c_j	concentration of component j (mol m^{-3})
$c_{j,0}$	theoretical initial concentration of component j in the reaction mixture (mol m^{-3})
c_p	heat capacity of the fluid ($\text{J kg}^{-1} \text{ K}^{-1}$)
d_h	hydraulic channel diameter (m)
E_A	activation energy of the reaction (J mol^{-1})
ΔH_R	enthalpy of reaction (J mol^{-1})
k	rate constant of the reaction, n th-order ($L^{n-1} \text{ mol}^{1-n} \text{ s}^{-1}$)
k_{1a}	volumetric mass-transfer coefficient (s^{-1})
K_p	distribution coefficient (dimensionless)
k_w	overall heat transfer coefficient ($\text{W m}^{-2} \text{ K}^{-1}$)
M_j	molar mass of component j (g mol^{-1})
\dot{n}_j	molar flow rate of component j (mol s^{-1})
$\dot{n}_{j,0}$	theoretical initial molar flow rate of component j (mol s^{-1})
r	reaction rate ($\text{mol m}^{-3} \text{ s}^{-1}$)
R	universal gas constant ($8.314 \text{ J mol}^{-1} \text{ K}^{-1}$)
t	time (s)
t'	dimensionless time $t' = t/t_r$
t_r	characteristic time scale of the reaction (s)
T	temperature (K)
T_w	wall temperature (K)
$\Delta T'$	dimensionless temperature difference

u	axial flow velocity (m s^{-1})
\dot{V}	volumetric flow rate ($\text{m}^3 \text{s}^{-1}$)
X_{MeIm}	conversion of 1-methylimidazole (dimensionless)
Y_{S}	yield of the bisazo dye 2,4-bis[(4-sulphophenyl)azo]-1-naphthol
z	axial distance from the reactor inlet (m)

Greek Symbols

ρ	density of the fluid (kg m^{-3})
--------	---

REFERENCES

- 1 D. A. Waterkamp, M. Heiland, M. Schlüter, J. C. Sauvageau, T. Beyersdorff and J. Thöming, Synthesis of ionic liquids in micro-reactors—a process intensification study, *Green Chem.*, 2007, **9**, 1084.
- 2 O. Levenspiel, *Chemical Reaction Engineering*, Wiley, New York, 1999.
- 3 A. Große Böwing and A. Jess, Kinetics of single- and two-phase synthesis of the ionic liquid 1-butyl-3-methylimidazolium chloride, *Green Chem.*, 2005, **7**, 230–235.
- 4 J. Baldyga, J. R. Bourne and B. Walker, Non-isothermal micromixing in turbulent liquids: Theory and experiment, *Can. J. Chem. Eng.*, 1998, **76**, 641–649.
- 5 J. R. Bourne, O. M. Kut, J. Lenzner and H. Maire, Kinetics of the diazo coupling between 1-naphthol and diazotized sulfanilic acid, *Ind. Eng. Chem. Res.*, 1990, **29**, 1761–1765.
- 6 J. Baldyga and J. R. Bourne, *Turbulent mixing and chemical reactions*, Wiley, New York, 1999.
- 7 S. Schwolow, J. Hollmann, B. Schenkel and T. Röder, Application-oriented analysis of mixing performance in microreactors, *Org. Process Res. Dev.*, 2012, **16**, 1513–1522.